Indian J. Phys. **75B (5)**, 397–402 (2001)

I J P B
— an international journal

Wide band spectral character *vis-a-vis* optical thickness of solar radio bursts

T K Das*, H Sarkar and G Tarafdar
Eastern Centre for Research in Astrophysics, Institute of Radiophysics & Electronics, 92, A P C Road, Kolkata-700 009, India
E-mail tusharkd@cucc ernet in

Received 3 April 2001, accepted 28 June 2001

Abstract Spectra of solar radio bursts observed simultaneously in some of the selected frequencies in the band 0.245–15.4 GHz (1.95–122.45 cm-λ), have been studied. The variation of spectral nature due to the variation of the magnetic field of the underlying active regions, and also due to the change in the heliographic position of the bursts on the solar disc, has been investigated as well. The directivity and the optical thickness have been found out in the aforesaid waveband after an extensive study on a large number of discrete events. An empirical relationship has been invoked for showing the variation of optical thickness with the observing wavelength of radio bursts occurring in the central region of the disk. From this relationship, it can be concluded that the variation of optical depth with the wavelength gives rise to a U-shaped pattern, attaining the minimum value around 1 GHz (30 cm-λ). A comparative study between the spectral nature and the optical thickness of solar radio bursts observed in a wide band of wavelengths, has been made in the present paper.

Keywords . Solar radio bursts, spectra, optical thickness

PACS No. 96.60.Rd

1. Introduction

Different kinds of work done on the spectral characteristics of solar radio bursts from meter to millimeter wave region have been presented in various excellent monographs published from time to time [1-4]. These spectra, the studies of which were concentrated mainly to the microwave region, were classified into several groups according to their spectral shape drawn on the basis of the observed peak flux measured with the help of receivers operating simultaneously in some selected frequencies. Different emission and absorption mechanisms were called into play in order to gain an insight into the physical characteristics of the ambient medium, where the radio emitting zones are located. But the actual emission measure of the source region is not obtained without the consideration of the attenuation caused simultaneously by the intervening medium during the period of burst event. So, in this present paper, we have made an attempt to get an idea about this emission measure in wide band of wavelengths from the experimentally observed data, after considering the effect of absorption in the respective band. In order to do this, we have drawn the wide band peak flux spectra of radio bursts, and subsequently, compared them with the degree of attenuation caused at different wavelengths, which has also been derived from a large number of experimental data.

2. Wide band spectral nature

Spectra of continuum type sporadic radio emission were drawn by taking burst-events having the characteristics of simultaneous multifrequency emission, each of which was reported by the same station, so that no error may creep into the measured flux values due to the use of different time constants of receivers and the differences or deficiencies of the calibration systems. These bursts (altogether 44 events) were observed at least at eight of the nine observing frequencies 0.245, 0.41, 0.606, 1.415, 2.695, 4.995, 8.8, 15.4, and 35 GHz by Sagamore Hill, Palehua, Learmonth, San Vito observatories during the period 1992–1994.

The peak flux values of a particular event in which the emission takes place in all the aforesaid frequencies in a

*Corresponding Author

simultaneous manner, were normalised with respect to the maximum value of peak flux observed for that event. After inspecting the spectral shape of each event, the spectra were grouped into several classes, each class giving a definite type of spectral nature. The averaging has been made only on those spectra in which the normalised values at a particular frequency do not deviate much from each other. In this way, the average spectra of the following kinds were obtained, which are illustrated in Figure 1.

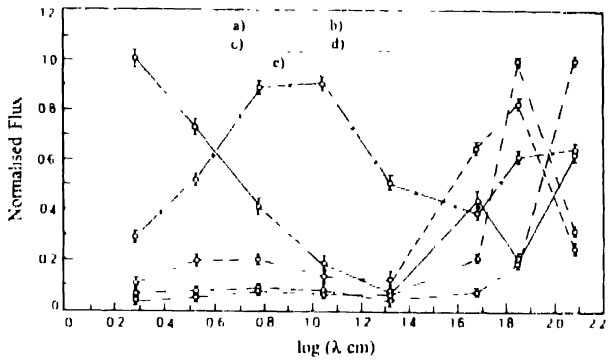

Figure 1. Wide band average spectra of radio bursts showing different types of spectral nature. The alphabets as shown in Figure represent the following types of spectra (a) U-shaped, (b) double peak, (c) inverted U, (d) flat and then increasing and (e) flat and peak at meterwave. The number of events on which the averaging has been done (a) 7, (b) 6, (c) 10, (d) 16 and (e) 5. Vertical lines give the estimated errors in the respective measured values.

(a) *U-shaped* : These spectra have a minima around 20 cm-λ (1.5 GHz) rising both in the higher and lower wavelength sides.

(b) *Double peak* : They possess the most prominent maxima around 75 cm-λ (0.4 GHz) and less prominent maxima around 4 cm-λ (7.5 GHz) with a dip in intensity around 20 cm-λ.

(c) *Inverted U* : They have broad peaks in the wavelength range 6–12 cm-λ (2.5–5 GHz), decreasing in the shorter wavelength side and increasing in the longer wavelength side with a dip in intensity around 50 cm-λ.

(d) *Flat and then increasing* : The spectra remain almost flat in the shorter wavelengths upto 30 cm-λ (1 GHz) and then they increase with the wavelength towards the longer wavelength above 30 cm-λ.

(e) *Flat with a peak at meterwave* : They remain flat upto 30 cm-λ, peaking around 75 cm-λ (0.4 GHz).

Out of these various types of spectra, the Inverted U and the Flat and then increasing types (3rd and 4th categories) are found to occur most (60% cases). Barring a few cases, the spectra either attain peak or have a tendency to attain peak in the longer wavelength region, elucidating that the radio emission becomes very much intense at meterwave band above 50 cm-λ. In the shorter wavelengths, the picture is different. In 60% cases, the spectral shape is either flat or gives a less pronounced peak in which the intensity value is about one fourth of that at meterwave. The dip in intensity, giving the spectral minima, generally occurs in the wavelength range 20–50 cm (0.6–1.5 GHz) in most of the cases studied.

3. Spectra at different magnetic fields

The burst-events were correlated with the underlying sunspot groups whose magnetic fields were given in some ranges. Most of the events (almost 80%) are found to be associated with active regions having magnetic field in the range 2100-3000 G. Figure 2 gives the spectra for the two ranges of

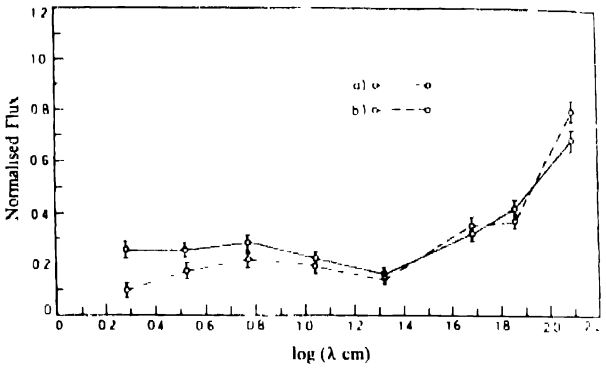

Figure 2. Normalised spectra of radio bursts for different ranges of magnetic field of associated active regions (a) represents field strength 1100-2000 G and (b) gives 2100–3000 G. The number of events taken for averaging (a) 9 and (b) 35.

magnetic field 1100-2000 G and 2100-3000 G. Higher the magnetic field, higher is the intensity at all wavelengths excepting the meterwave region. Again, the gap between the two curves increases more and more, as the shorter wavelength is approached, which indicates the predominant role of magnetic field in the emissivity in the microwave region.

4. Spectral variation due to the different location of bursts

The location of a burst was identified by the respective position of the associated Hα-flares. The radio bursts and Hα-flares were regarded for association, when their starting times did not differ more than ±5 min from each other. According to the position on the solar disc, the spectra were grouped into the following categories :

(i) Limb bursts : position in the 61-90° longitude,

(ii) Mid bursts : having location 31-60° longitude,

(iii) Central bursts : having location 0-30° longitude.

From Figure 3(i), it is evident that the intensity of limb bursts is greater than those of central and mid bursts at all the wavelengths below 100 cm-λ. When the central and mid region bursts are compared, it is observed that the central

bursts are more intense than the mid bursts in the shorter wavelengths below 20 cm-λ and the reverse is true for the

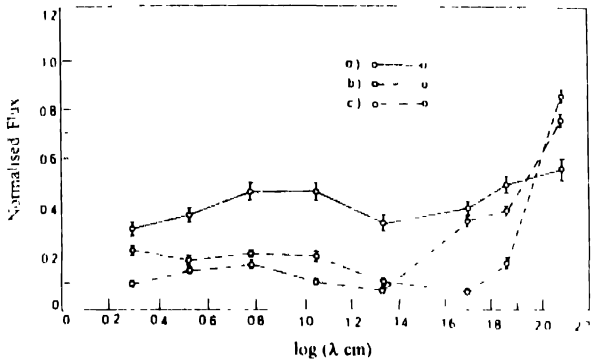

Figure 3(i). Centre to limb variation of spectral nature (a) represents limb bursts (61° 90° longitude), (b) central bursts (0°–30°) and (c) mid longitude bursts (31°–60°) The number of events taken for averaging (a) 16, (b) 6 and (c) 22

wavelengths above 20 cm. Figure 3(ii) gives the anisotropy in the intensity of radio bursts occurring at the mid latitude and limb regions with respect to the central bursts

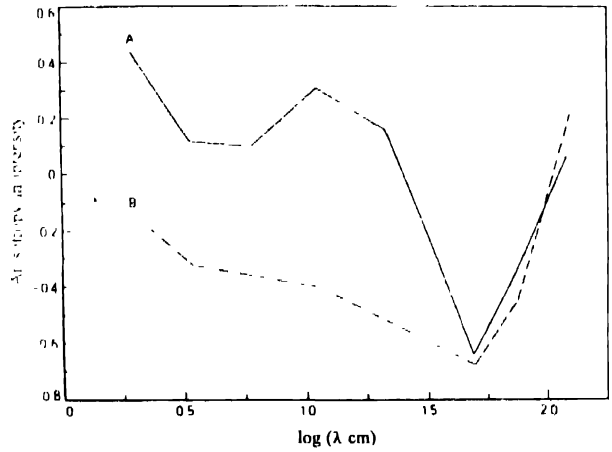

Figure 3(ii). Longitude dependence of the anisotropy in the intensity of radio bursts (A) for mid latitude bursts and (B) for limb bursts

These results are now compared with those of earlier reports. Kakinuma *et al* [5] obtained the intensity ratio $F(60°-90°)/F(0°-30°)$ varying in the range 0.6–0.7 at all frequencies between 1 GHz and 9.4 GHz; while Scalise and coworkers [6,7] obtained the ratio $F(60°-90°)/F(0°-15°)$ as 1.5 at 9.4 GHz, 0.7 at 3.75 GHz, 1 at 2 GHz and 1.5 at 1 GHz. Gelfrick [8] reported the results of observations with the RATAN 600 which comply with our present study as well as with the prediction based on a homogeneous model of solar atmosphere.

5. Intensity distribution of radio bursts

In order to find out the actual intensity distribution of radio bursts observed in the frequency range 0.245–15.4 GHz, the burst intensity should assume all the values ranging from zero to infinity. For this reason, we have taken a large number of radio bursts in each of the aforesaid frequencies as shown in Table 1. The occurrence frequency distribution of the intensity of radio bursts at different frequencies has been reported in our earlier paper [9] and is given by

$$\frac{\Delta N}{\Delta I} = aI^b e^{-c(\ln I)^2}, \tag{1}$$

where ΔN represents the number of bursts in the intensity range I to $(I + \Delta I)$ and a, b and c are arbitrary contents. The values of these constants are displayed in Table 1.

Table 1. Values of different constants at different frequencies

Frequency of observation in GHz	Total number of bursts	Values of constants		
		b	c	σ
0 245	2730	1 25	0 23	67 9
0 410	2008	0 44	0 19	62 9
0 650	1665	−1 22	0 04	72.1
0 950	1216	−1 25	0 04	79 4
2 800	2027	1 65	0 02	44 98
4 995	2240	0 21	0 15	63 90
8 800	1888	0 79	0 20	59 20
15 400	1600	0 67	0 19	70 80

With the help of this sort of newly devised distribution law, the optical thickness of the absorbing layer has been found out at different frequencies of radio bursts after examining their directivity that is thought to be due to the attenuation caused by the absorbing layer above the burst source [10].

6. Directivity of radio bursts at various wavelengths

In order to find out the directivity of radio bursts, the occurrences of bursts (ΔN) in different ranges of angular widths ($\Delta\theta$) have been found out and $\Delta N/\Delta\theta$ have been calculated and plotted against θ which represents the mid-value of the respective range. It has been found that the angular distribution can be fitted with a Gaussian distribution of the following type :

$$f(\theta) = \frac{\Delta N}{\Delta\theta} = f(0)\exp\left[\frac{(\theta-\bar{\theta})^{-2}}{2\sigma^2}\right.$$

and $$f(0) = \left[\frac{\Delta N}{\Delta\theta}\right]_{\theta=0}, \tag{2}$$

where θ varies from $-\pi/2$ to $\pi/2$.

It has been found from the data that $\bar{\theta} \simeq 0$.

$$\text{So, } f(\theta) = f(0)\exp\left[-\frac{\theta^2}{2\sigma^2}\right]. \tag{3}$$

$$\text{Hence, } \ln\frac{\Delta N}{\Delta\theta} = \ln f(0) - \frac{\theta^2}{2\sigma^2}. \tag{4}$$

The plots of ln $\Delta N/\Delta\theta$ against θ^2 are shown in Figure 4. The slope of each of the straight lines gives the value of $1/2\sigma^2$ from which σ has been found out. The value of σ gives a

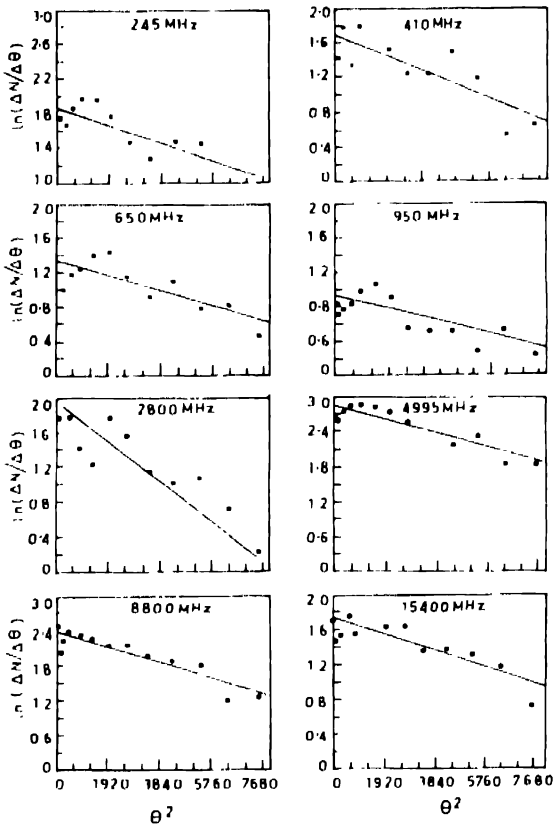

Figure 4. Plots of ln $\Delta N/\Delta\theta$ against θ^2. The slope of the straight line gives the value of $1/2\sigma^2$ in each of the observing frequencies.

measure of dispersion of the data in different locations on the disk at a particular frequency. The computed values of σ are shown in Table 1. It is observed that the dispersion attains a minimum around 3 GHz (10 cm-λ) and maximum around 1 GHz (30 cm-λ).

As the dispersion is least around 10 cm-λ, it can be concluded that most of the bursts at this frequency are centrally located, *i e*, maximum number of bursts in this frequency may be called central bursts.

7. Optical thickness at different wavelengths for central bursts

Let us consider a parallel plane layer model of the solar atmosphere. The attenuation is caused by the absorbing layer above the source of a burst. When it is observed along a line inclined at an angle θ with the direct line of sight, the observed intensity becomes $Ie^{-\Delta\tau}$, where I is the intensity of the source located at the origin and $\Delta\tau = \tau - \tau_0$. Here, τ is the optical thickness along the inclined line of sight and τ_0 along the direct line of sight.

Hence, $$\Delta\tau = \tau - \tau_0 = \tau_0(\sec\theta - 1). \qquad (5)$$

So the number of bursts observed along the line at an angle θ with respect to the direct observation is

$$N(\theta) = \int_{I_{\min}e^{\Delta\tau}}^{\infty} dN. \qquad (6)$$

Taking the minimum value of intensity $I_{\min}$ as 1 s.f.u., it can be written as

$$N(\theta)/N(0) = erfc\left[\sqrt{c}(\ln I_{\min} + V\tau - (b+1)/2c)\right]/ erfc\left[\sqrt{c}(\ln I_{\min} - (b+1)/2c)\right].$$

This ratio can be equated to $f(\theta)/f(0)$ obtained from eq. (3).

$$erfc\left[\sqrt{c}(\ln I_{\min} + V\tau - (b+1)/2c)\right]/erfc \times \left[\sqrt{c}(\ln I_{\min} - (b+1)/2c)\right] = -\theta^2/2\sigma^2. \qquad (7)$$

For $\theta = 0$, $\tau = \tau_0$, hence $\Delta\tau = 0$.

For evaluating $\Delta\tau$ in each frequency, the eq. (7) has been used and the corresponding values of the constants b, c and σ have been obtained from Table 1.

From the eq. (7), the values of $\Delta\tau$ have been computed on the basis of the statistical analyses obtained from the intensity distribution as well as from the longitudinal distribution of the observed radio bursts. These $\Delta\tau$ values have been plotted against (sec θ–1) as shown in Figure 5. The Figure shows that the values of $\Delta\tau$ increase with

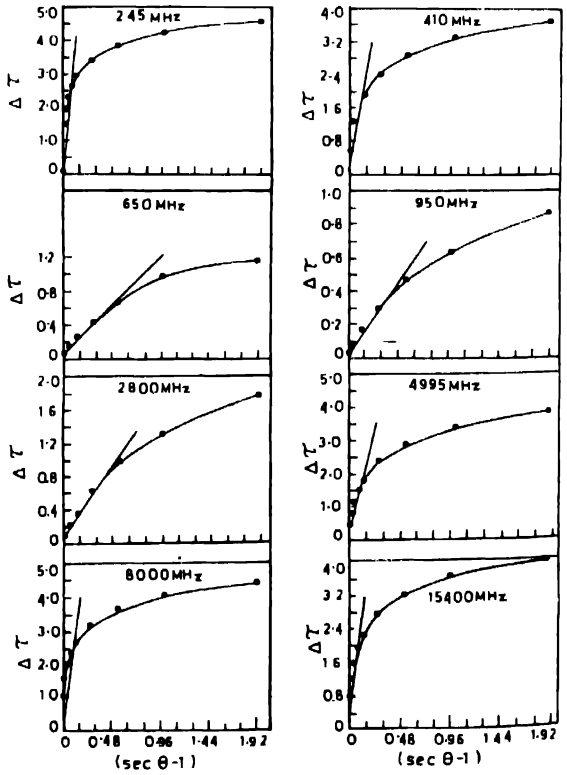

Figure 5. Curves showing the variation of $\Delta\tau$ against (sec θ–1).

(sec θ - 1) almost exponentially passing through origin. Upto 30° all the curves are approximately linear excepting the frequencies 0.65, 0.95 and 2.8 GHz for which the linearity extends upto 50°. Taking the linear portion which passes through the origin, we have, in this analysis, calculated the values of τ_0 assuming that $\Delta\tau$ varies linearly with (sec θ 1) as shown in eq. (5). Hence, the slopes of the straight lines give the values of τ_0 at different frequencies.

After finding out the values of τ_0, a graph as shown in Figure 6 is drawn against τ_0 (in neper) *versus* $\log_{10}\lambda$ (in cm).

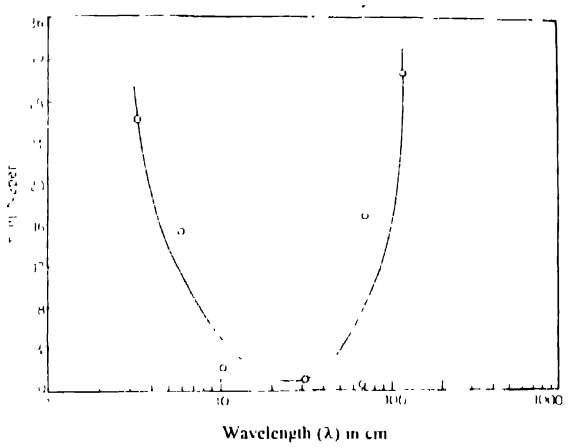

Figure 6. The curve gives the variation of τ_0 against $\log\lambda$ from which the dependence of τ_0 on the wavelength λ is derived

The optical thickness as obtained from the best fitting curve for the whole range of frequency under consideration is given as follows :

$$\tau_0 = 1.2\times10^{-4}\lambda^{2.6} + 192.4\lambda^{-1.6}. \quad (8)$$

The correlation coefficient between the statistically obtained values of τ_0 based on experimentally observed radio burst data and the computed values from this empirical relation (8) is about 0.925, showing the best fit between them

Thus, the optical thickness τ_0 for the central bursts attains the minimum value at around 1 GHz (30 cm-λ), but it increases with the decrease as well as the increase of wavelength. In the lower wavelength side, the values of τ_0 derived from the empirical relation fit well with those of the earlier workers [2,11] who reported that the optical thickness of the corona read from the level (R^*) where the refractive index is zero, rises as the wavelength decreases This is connected with the corresponding displacement of the reflecting layer into the deeper layers of the corona and then the chromosphere with higher electron density (N^2) values and a lower temperature T. As a result of this, the coefficient of reflection of electromagnetic waves from the solar atmosphere falls as λ decreases ($e^{-2\pi R^*}$).

In the longer wavelength side (coronal region), the free-free opacity is given as [4] :

$$\tau_{ff} \propto \lambda^2 \sec\theta, \quad (9)$$

where θ is the angular distance from the Sun's centre. Taking θ 0 for the central bursts, it can be written as

$$\tau_{ff} \propto \lambda^2. \quad (10)$$

Again, from the eq. (8), it is evident that for greater wavelengths, the first term dominates over the second one, the exponent of this term being equal to 2.6 In eq. (10), the optical thickness has been considered on the basis of free-free absorption only, but other kinds of absorption effects [3,12 15], like absorption below plasma frequency, gyro-resonance absorption, gyro-synchrotron re-absorption by the radiating electrons themselves and Razin-Tsytovich effect are to be taken into consideration for getting a true picture of the optical depth.

It is observed that the optical thickness for the central bursts is minimum around 30 cm-λ. In comparison to 10 cm-λ bursts, the 30 cm-λ bursts have lower directivity which is nothing but the reciprocal of the variance σ, and also they have the least optical thickness. So the various absorption phenomena thought to be prevalent in the solar atmosphere, play the least role on the emitted radiation, as a result of which the radiation is least suppressed.

8. Discussions and conclusion

From the foregoing analysis, it is observed that in the shorter-wavelength region, the spectrum is either flat or possesses a less prominent peak compared to that at meterwave region. In this wave band, the optical thickness is found to be high, which corroborates the earlier reports as well; the results are found to fit quite well with the shape of the spectra obtained from the present study Around 30 cm-λ, the spectral intensity is minimum, *vis-à-vis*, the optical thickness is also minimum. In the meterwave region, the spectral intensity attains the highest possible value in most of the events; in tune with this, the optical thickness approaches larger values at greater wavelengths. For larger wavelengths above 50 cm-λ (below 0.6 GHz), the actual emission measure of the radio sources might be more high enough, so that, in spite of greater attenuation caused by the absorbing layer, the observed emission intensity becomes considerably higher than that of the microwave part of the spectrum. This may be due to the fact that the emission at metric-decimetric waves come from regions higher in the corona and are originated by a number of emission mechanisms, such as, plasma waves excited by particle beams, or shock waves.

In examining the intensity distribution of radio bursts as given by eq. (1), no consideration has been made about the center-to-limb dependence of circular polarisation which may influence the total flux determinations. As the data used in this analysis were obtained with the help of linearly polarised telescopes, hence, some error may creep into the empirical relation obtained so far. Moreover, the frequency band used in this analysis covers the metrewave as well as the microwave band, and hence, the emission mechanisms

differ for the different parts of the radio spectrum. All these processes have their respective self absorption coefficients which could not be taken into consideration for evaluating the optical thickness because of the paucity of the relevant data. But whatever may be the absorption mechanisms, the directivity of bursts may be used as a yardstick for the determination of optical thickness in the entire band of wavelengths.

References

[1] M R Kundu *Solar Radio Astronomy* (New York Interscience) (1965)

[2] V V Zheleznyakov *Radio Emission of the Sun and Planets* (Oxford Pergamon) (1970)

[3] D J McLean and N R Labrum *Solar Radiophysics* (Cambridge Cambridge University Press) (1985)

[4] H Zirin *Astrophysics of the Sun* (Cambridge Cambridge University Press) (1989)

[5] T Kakinuma, T Yamashita and S Enome *Proc. Res Inst Atmospherics* (Nagoya Univ.) p16 (1969)

[6] E Scalise (Jr) *Publ Astron Soc. Jpn* (1970)

[7] T Takakura and E Scalise (Jr) *Solar Phys* **11** 434 (1970)

[8] G B Gelfrick *Proc Work Sol Electro Rad. Study Sol Cycle 22* (ed) R F Donnelly (U S Dept. Com., NOAA) p196 (1992)

[9] T K Das, G Tarafdar and A K Sen *Solar Phys* **176** 181 (1997)

[10] K Akabane *Publ Astron Soc Jpn* **8** 173 (1956)

[11] S F Smerd *Aust J Sci Res.* **A3** 34 (1950)

[12] M K Das Gupta, I K Das and S K Sarkar *Solar Phys* **67** 109 (1980)

[13] T Takukura *Solar Phys* **1** 304 (1967)

[14] R Ramaty *Astrophys J* **158** 753 (1969)

[15] R Ramaty *High Energy Phenomena on the Sun* eds Ramaty and P G Stone (NASA SP-342) p188 (1973)